Neutron spectroscopic determination of the crystalline electric field in $HoBa_2Cu_3O_{7-\delta}$

A. Furrer
Labor für Neutronenstreuung, Eidgenössische Technische Hochschule Zürich, CH-5303 Würenlingen, Switzerland

P. Brüesch and P. Unternährer
Asea Brown Boveri Corporate Research, CH-5404 Baden, Switzerland
(Received 22 April 1988)

Inelastic neutron scattering has been employed to study the crystalline electric field (CEF) interaction in the high-T_c superconductor $HoBa_2Cu_3O_{7-\delta}$. The CEF at the Ho site completely lifts the 17-fold degeneracy of the ground-state J multiplet. The observed energy spectra exhibit a large number of well-resolved CEF transitions between 0.5 and 73 meV, so that we have been able to assign the energies of ten excited CEF levels. On the basis of the observed intensities we have been able to unambiguously determine all nine CEF parameters required for orthorhombic symmetry. The CEF parameters turn out to be incompatible with any kind of point-charge calculation as expected. The results are used to predict the magnetization and the field-dependent Schottky anomaly of the heat capacity of $HoBa_2Cu_3O_7$ as well as to extrapolate the CEF interaction to $ErBa_2Cu_3O_7$, which yields good agreement with the experimental data.

I. INTRODUCTION

The recent discovery of high-T_c superconductivity in the perovskite La-(Ba,Sr)-Cu-O and (Y,La)-Ba-Cu-O systems[1,2] has given rise to a large amount of materials research. Of particular interest in determining the nature of the superconductivity is the effect of substituents at various sites in these compounds. It has been realized that the superconducting transition temperature is essentially unchanged upon replacing the Y and La ions by "magnetic" lanthanide ions.[3-5] This is in contrast to conventional superconductors, for which paramagnetic ions usually have a large detrimental effect on superconductivity. However, since the superconductivity in the perovskite-type systems must be most likely associated with the copper-oxygen planes, this is not really a surprising result. We may therefore anticipate an almost uncorrelated coexistence of superconductivity and magnetism in the copper-oxygen and lanthanide layers, respectively, which is nicely illustrated by the observation of two-dimensional antiferromagnetic ordering in $ErBa_2Cu_3O_7$ below $T_N = 0.5$ K (Ref. 6) and $HoBa_2Cu_3O_7$ below $T_N = 0.14$ K.[7] On the other hand, the recent discovery of three-dimensional antiferromagnetic ordering in $GdBa_2Cu_3O_7$ below $T_N = 2.22$ K (Ref. 8) and $DyBa_2Cu_3O_7$ below $T_N = 1$ K,[7,9] raises the interesting question of how the magnetic interactions succeed in transversing the copper-oxygen layers without influencing the superconducting state. So far the basic differences in the magnetic ordering of the above-mentioned compounds are not understood, but it is clear that crystalline electric field (CEF) effects may play the key role in determining the magnetic ground state.

Very detailed information about the CEF interaction results from inelastic neutron scattering (INS) experiments. There has been a considerable effort to study the CEF interaction in the $RBa_2Cu_3O_7$ (R denotes rare earth) compounds by the INS technique,[10-14] but none of these efforts have resulted in a quantitative understanding in terms of detailed CEF parameters, and consequently the nature of the magnetic ground state, i.e., the wave functions of the CEF states, remained unknown. This is due to the low symmetry of the CEF potential (orthorhombic site symmetry D_{2h}) which is determined by nine independent CEF parameters. Thus an unambiguous determination of the CEF interaction requires the observation of at least nine different excited CEF states which can hardly be achieved for most of the $RBa_2Cu_3O_7$ compounds.

In this paper we present INS experiments on $HoBa_2Cu_3O_{7-\delta}$. We have particularly chosen this compound, since it has the largest number of CEF states among the rare-earth series. The 17-fold degeneracy of the ground-state J multiplet is completely lifted by the CEF. From our observations we have been able to unambiguously determine all nine CEF parameters required for orthorhombic symmetry, so that we arrived at a detailed understanding of the magnetic ground state. Our results are discussed and used to calculate various thermodynamic magnetic properties of $HoBa_2Cu_3O_7$ which are found to be in good agreement with the experimental data. A preliminary account of the present work was given in Ref. 15.

II. EXPERIMENT

The $HoBa_2Cu_3O_{7-\delta}$ sample was the same as that used in Ref. 7. It was prepared by mixing powders of Ho_2O_3 (>99.9%), BaO_2 (>95%), and CuO (>99.9%) in stoichiometric proportions according to the formula $HoBa_2Cu_3O_{6.5}$ for 1 h under hexane. The mixture was heated to 950 °C at a rate of 320 °C/h, maintained at 950 °C for 19 h in oxygen and quenched. The calcined

mixture was ground under hexane for 3 h. The mixture was then reheated to 950 °C and cooled to room temperature in oxygen at a rate of 16 °C/h. The mixture was reground under hexane for 1 h (grain size < 32 μm). The resulting powder was pressed into pellets at a pressure of 300 MPa. The pellets were heated to 950 °C at a rate of 350 °C/h, maintained at 950 °C for 2 h under oxygen, and cooled under oxygen to room temperature at a rate of 40 °C/h. The density of the pellets was 89.3% of the crystallographic density.

The sample satisfied the levitation criterion and showed a sharp drop in resistivity at $T_c = 93.5$ K (midpoint) with $\Delta T_{10-90} \leq 1$ K. The oxygen deficiency δ was determined by neutron diffraction,[7] thermogravimetry, and an iodometric titration technique.[16] The former method gave $\delta = 0.22 \pm 0.06$, while the latter two methods gave $\delta = 0.13 \pm 0.05$ and $\delta = 0.12 \pm 0.05$, respectively. Neutron-diffraction experiments[7] proved the single-phase character of the sample.

The INS experiments were performed at the reactor Saphir in Würenlingen on the triple-axis spectrometer R5 operated in the neutron energy-loss configuration. The energy of the scattered neutrons was kept fixed either at 5 meV or at 13.7 meV, giving rise to energy resolutions ($\hbar\omega = 0$) of 0.2 and 1.2 meV, respectively. To gain intensity the measurements were carried out with use of a doubly bent graphite monochromator as well as a horizontally bent graphite analyzer, both with (002) scattering planes. Pyrolitic graphite or beryllium filters were inserted into the outgoing neutron beam to reduce higher-order contamination. The experiments were performed for moduli of the scattering vector Q and temperatures in the ranges $1.1 \leq Q \leq 5.5$ Å^{-1} and $1.5 \leq T \leq 100$ K, respectively. The $HoBa_2Cu_3O_{7-\delta}$ pellets were powdered and enclosed into a cylindrical aluminum container of 15 mm diameter and 50 mm height.

III. RESULTS

The energy spectra taken at $T = 1.5$ K exhibit seven well-resolved inelastic lines in a low-energy window ($\hbar\omega < 12$ meV) and in a high-energy window ($55 < \hbar\omega < 75$ meV) as shown in Fig. 1. The gap between the two windows is almost completely structureless. We can immediately interpret all seven lines in terms of

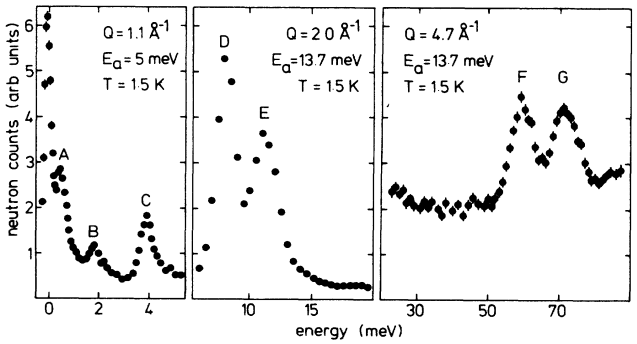

FIG. 1. Energy spectra of neutrons scattered from $HoBa_2Cu_3O_{7-\delta}$ at 1.5 K. E_a denotes the analyzer energy.

CEF transitions out of the ground state, since none of the excited CEF states are sufficiently populated at 1.5 K and the phonon density of states of the "nonmagnetic" reference compound $YBa_2Cu_3O_7$ essentially exhibits a single inelastic line at around 20 meV.[17] Thus the phonon contributions to the energy spectra are outside the low- and high-energy windows mentioned above, and the phonon intensities are at least an order of magnitude smaller than the CEF transitions as evidenced by Fig. 1. Moreover, CEF transitions can readily be identified by the way in which their intensities vary with temperature and scattering vector. For noninteracting ions the differential neutron cross section for the CEF transition $|\Gamma_i\rangle \rightarrow |\Gamma_j\rangle$ is given in the dipole approximation by[18]

$$\frac{d^2\sigma}{d\Omega\, d\omega} \sim F^2(Q) \exp\left(\frac{-E_i}{k_B T}\right) |\langle \Gamma_j | J_\perp | \Gamma_i \rangle|^2 \times \delta(E_i - E_j + \hbar\omega) , \quad (1)$$

where $F(Q)$ is the magnetic form factor, E_i the energy of the ith CEF state with irreducible representation Γ_i, and $J_\perp$ the component of the total angular momentum operator perpendicular to the scattering vector Q. Thus the intensities of CEF transitions are decreasing with increasing scattering vector due to the form factor, and their temperature dependences are governed by Boltzman statistics, whereas phonon intensities usually increase with increasing scattering vector (apart from the modulation due to the structure factor) and their temperature dependences follow Bose statistics. Typical energy spectra demonstrating the Q and T dependences of the observed CEF transitions are shown in Figs. 2–5.

We now consider the CEF transitions A,B,C of Fig. 2 in detail. The Q dependences are clearly in agreement with the form factor. The peak intensities A and B decrease by typically 20% upon raising the temperature from 1.5 to 4.2 K as expected for ground-state CEF transitions, whereas peak C roughly retains its intensity. Obviously a CEF transition out of the first-excited CEF state accidentally coincides with a ground-state CEF transition at the energy of the peak position C. We therefore identify from Fig. 2 excited CEF states at 0.5 meV (peak A), 1.8 meV (peak B), 3.8 meV (peak C), and 4.3 meV (peak C). The high-energy shoulders of the peaks B and C will be discussed in Sec. IV.

Figure 3 confirms our interpretation of peak C as well as the magnetic origin of peaks D and E through a detailed inspection of their intensities as a function of both temperature and momentum transfer. The linewidths of peaks C and D correspond to the instrumental energy resolution, whereas peak E appears to be considerably broader, i.e., peak E is the result of a superposition of at least two ground-state CEF transitions with slightly different energies. Indeed a Gaussian fit to the 1.5-K spectrum gives evidence for further excited CEF states at 8.1 meV (peak D) and at 11.2 ± 0.4 meV (peak E) as shown in Fig. 3.

A detailed identification of CEF transitions in the high-energy window becomes more difficult for various reasons. First, the energy resolution for high-energy transfers is rather poor in conventional INS experiments.

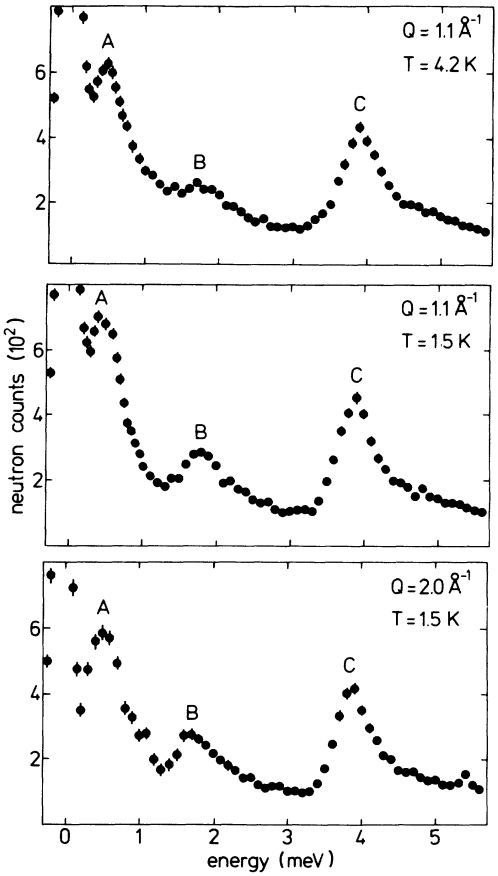

FIG. 2. Energy spectra of neutrons scattered from $HoBa_2Cu_3O_{7-\delta}$ for $E_a = 5$ meV.

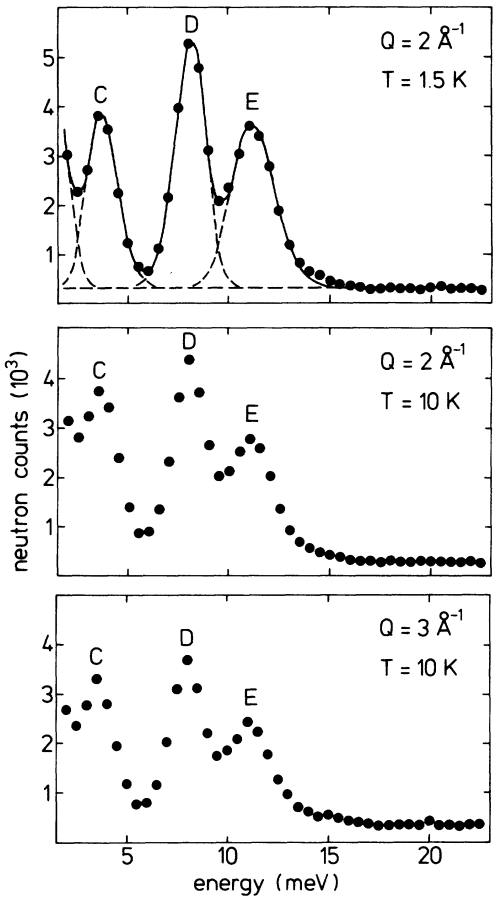

FIG. 3. Energy spectra of neutrons scattered from $HoBa_2Cu_3O_{7-\delta}$ for $E_a = 13.7$ meV. The curves are described in the text.

Second, kinematical constraints restrict the accessible Q range to rather high values where the form factor flattens out and can no longer be used to discriminate between phonons and CEF excitations. Third, the energy spectra taken at high temperatures become smeared out due to the rapidly increasing number of excited CEF transitions. The latter effect is readily visualized in Fig. 4. Only at 1.5 K are peaks F and G well resolved. Peak G is considerably broader than the instrumental energy resolution, and we conclude that at least two ground-state CEF transitions contribute to its intensity. This interpretation is supported by a Gaussian least-squares fit, so that we identify further excited CEF states at 59 meV (peak F) and at 71.5 ± 1.5 meV (peak G).

We have also performed INS experiments above T_c. Typical energy spectra are shown in Fig. 5. The main features of the CEF excitation spectra observed at low temperatures are still present, but the energy spectra are considerably contaminated by excited CEF transitions, so that a straightforward analysis in terms of peak positions is no longer feasible.

IV. ANALYSIS OF RESULTS

The degeneracy of the J multiplets of a magnetic ion embedded in a crystal lattice is partly removed by the CEF potential produced by the charge distribution of the surrounding ions. In rare-earth compounds the CEF interaction is generally much smaller than the spin-orbit interaction, and in most cases the separation between adjacent J levels exceeds the overall CEF splitting by at least an order of magnitude, so that the CEF potential may be represented as a perturbation of the ground-state J multiplet alone. The corresponding Hamiltonian for the orthorhombic symmetry D_{2h} of Ho^{3+} in $HoBa_2Cu_3O_7$ is given by

$$\mathcal{H}_{\mathrm{CEF}} = \sum_{n=1}^{3} \sum_{m=0}^{n} B_{2n}^{2m} O_{2n}^{2m}, \tag{2}$$

where the B_{2n}^{2m} denote the CEF parameters and the O_{2n}^{2m} are operator equivalents built up by spin operators.[19]

The CEF Hamiltonian (2) gives rise to a complete decomposition of the ground-state J-multiplet $^5I_8$ of Ho^{3+} in $HoBa_2Cu_3O_7$ into 17 states Γ_i, namely $5\times\Gamma_1$, $4\times\Gamma_2$, $4\times\Gamma_3$, and $4\times\Gamma_4$. The wave functions of the irreducible representations Γ_i are given by

$$|\Gamma_i\rangle = \sum_{M=-J}^{J} a_M^i |M\rangle, \tag{3}$$

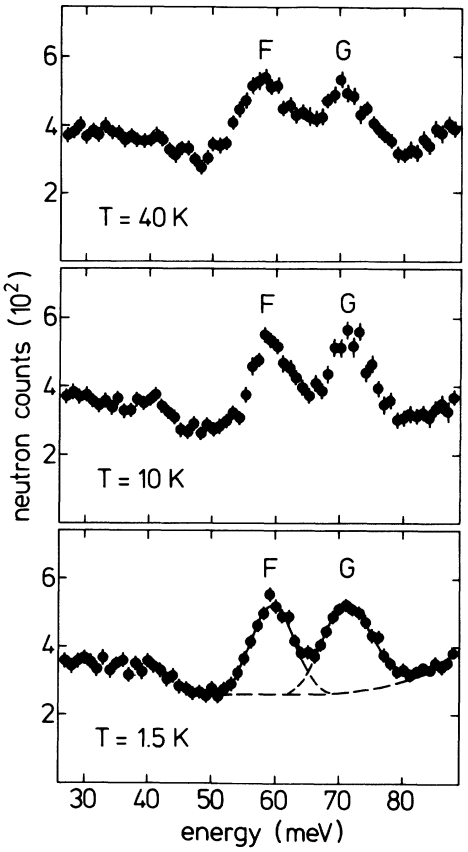

FIG. 4. Energy spectra of neutrons scattered from $HoBa_2Cu_3O_{7-\delta}$ for $Q=4.7$ Å^{-1} and $E_a=13.7$ meV. The curves are described in the text.

which obey the following symmetry relations:

$$
\begin{aligned}
|\Gamma_1\rangle &= a_8|8\rangle+a_6|6\rangle+a_4|4\rangle+a_2|2\rangle+a_0|0\rangle \\
&\quad +a_2|-2\rangle+a_4|-4\rangle+a_6|-6\rangle+a_8|-8\rangle, \\
|\Gamma_2\rangle &= a_7|7\rangle+a_5|5\rangle+a_3|3\rangle+a_1|1\rangle+a_1|-1\rangle \\
&\quad +a_3|-3\rangle+a_5|-5\rangle+a_7|-7\rangle, \\
|\Gamma_3\rangle &= a_8|8\rangle+a_6|6\rangle+a_4|4\rangle+a_2|2\rangle+0|0\rangle \\
&\quad -a_2|-2\rangle-a_4|-4\rangle-a_6|-6\rangle-a_8|-8\rangle, \\
|\Gamma_4\rangle &= a_7|7\rangle+a_5|5\rangle+a_3|3\rangle+a_1|1\rangle-a_1|-1\rangle \\
&\quad -a_3|-3\rangle-a_5|-5\rangle-a_7|-7\rangle.
\end{aligned}
\tag{4}
$$

From Eq. (4) we can readily calculate the transition matrix elements of Eq. (1), and we find the following selection rules for CEF transitions:

$$
\begin{aligned}
&\langle\Gamma_j|J_\perp|\Gamma_i\rangle\neq 0, \\
&\langle\Gamma_i|J_\perp|\Gamma_i\rangle=0.
\end{aligned}
\tag{5}
$$

Thus we have 12 or 13 allowed ground-state transitions depending on whether the CEF ground state is Γ_1 or $\Gamma_i\neq\Gamma_1$, respectively. In the present INS experiments we have been able to observe the majority of the allowed CEF ground-state transitions as well as to assign the energies of

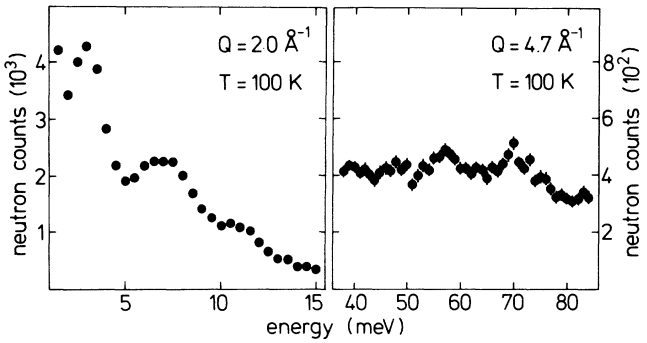

FIG. 5. Energy spectra of neutrons scattered from $HoBa_2Cu_3O_{7-\delta}$ at 100 K for $E_a=13.7$ meV.

ten among the 16 excited CEF levels, which is sufficient to determine the nine disposable CEF parameters of the Hamiltonian (2). However, since there is no *a priori* information on the CEF parameters B_{2n}^{2m}, an unambiguous interpretation of the observed energy spectra is not at all straightforward. In fact, to our knowledge there exist no detailed analyses of INS spectra of similar low-symmetry systems in the current literature so far. The most difficult problem of any nonlinear least-squares fitting procedure is a reasonable choice of the start values of the fitting parameters, which we have been able to assign as described below.

The coordination polyhedra of Ho^{3+} in $HoBa_2Cu_3O_7$ formed, e.g., by the eight nearest oxygen neighbors or by the eight nearest copper neighbors are slightly distorted cubes. Thus we expect the overall features of the CEF potential in a first approximation to be reasonably described by cubic symmetry, which considerably limits the number of disposable CEF parameters. For a cubic CEF we have $B_4^4=\pm 5B_4^0\neq 0$, $B_6^4=\mp 21B_6^0\neq 0$, $B_2^0=B_2^2=B_4^2=B_6^2=B_6^6=0$, i.e., the CEF interaction is determined by only two independent CEF parameters. The raising of the degeneracy of J multiplets by a cubic CEF has been worked out in detail by Lea, Leask and Wolf (LLW).[20] Now we make use of the particular features of the energy spectra observed for $HoBa_2Cu_3O_7$, which separate the CEF states into a low- and high-energy window (see Fig. 1). This can only be realized for the LLW parameter $x\simeq -0.45$ (see Fig. 1 in Ref. 20), so that we are able to roughly estimate the nonvanishing fourth- and sixth-order CEF parameters which finally constitute the dominant terms in the orthorhombic CEF potential (2) of $HoBa_2Cu_3O_7$. In a second step we have made use of the fact that from general experience with CEF problems the ratios of the CEF parameters B_{2n}^{2m} for a particular degree $2n$ may reasonably be determined by taking account of the geometry of the nearest-neighboring coordination polyhedra:

$$
\begin{aligned}
&B_2^2=\frac{\gamma_2^2}{\gamma_2^0}B_2^0, \\
&B_4^2=\frac{\gamma_4^2}{\gamma_4^0}B_4^0,\quad B_4^4=\frac{\gamma_4^4}{\gamma_4^0}B_4^0, \\
&B_6^2=\frac{\gamma_6^2}{\gamma_6^0}B_6^0,\quad B_6^4=\frac{\gamma_6^4}{\gamma_6^0}B_6^0,\quad B_6^6=\frac{\gamma_6^6}{\gamma_6^0}B_6^0.
\end{aligned}
\tag{6}
$$

The coordination factors γ_{2n}^{2m} as defined, e.g., by Hutchings[21] are listed in Table I for the nearest-neighbor oxygen and copper coordination polyhedra. Using these constraints we are left with three independent CEF parameters B_2^0, B_4^0, B_6^0. In order to cover all possible ratios B_4^0/B_2^0 and B_4^0/B_6^0 we used the following parametrization scheme:

$$\frac{B_4^0}{B_2^0}=\frac{xy}{30(1-|y|)}, \qquad \frac{B_4^0}{B_6^0}=\frac{231x}{1-|x|}, \tag{7}$$

with $-1\le x\le 1$ and $-1\le y\le 1$. We found a variety of parameter sets x,y which roughly predict the energies of the ten observed excited CEF levels; however, for only one parameter set we also obtained reasonable agreement with the observed intensities of the corresponding CEF transitions, namely for $x\simeq -0.4$ (as expected from the above-mentioned cubic approximation), $y\simeq 0.6$ and nearest-neighbor oxygen coordination; the nearest-neighbor copper coordination failed to provide agreement between the observed and calculated intensities. After having determined the most reasonable start values of the CEF parameters in such a manner, a least-squares-fitting procedure was performed in which all nine CEF parameters were allowed to vary independently. Perfect convergence was achieved for the following CEF parameters:

$$\begin{aligned}
B_2^0&=(-4.6\pm 0.2)\times 10^{-2}\ \text{meV},\\
B_2^2&=(-2.0\pm 0.4)\times 10^{-2}\ \text{meV},\\
B_4^0&=(9.1\pm 0.1)\times 10^{-4}\ \text{meV},\\
B_4^2&=(-0.6\pm 0.2)\times 10^{-4}\ \text{meV},\\
B_4^4&=(-4.2\pm 0.1)\times 10^{-3}\ \text{meV},\\
B_6^0&=(-4.5\pm 0.1)\times 10^{-6}\ \text{meV},\\
B_6^2&=(2.7\pm 0.8)\times 10^{-6}\ \text{meV},\\
B_6^4&=(-1.35\pm 0.02)\times 10^{-4}\ \text{meV},\\
B_6^6&=(1.9\pm 0.7)\times 10^{-6}\ \text{meV}.
\end{aligned} \tag{8}$$

The calculated CEF level scheme is shown in Fig. 6 and in Table II, which is in excellent agreement with the observations. Table II also lists the matrix elements of all the ground-state CEF transitions which are in reasonable agreement with the observed intensities, typically within 10–20%. The wave functions of the CEF states given in Table II will be important to calculate the magnetic properties of $HoBa_2Cu_3O_7$; see Sec. V.

We have not attempted to perform profile fits to the observed energy spectra for the following reason. Some of the observed CEF transitions appear to be asymmetric as, e.g., evidenced for the peaks B and C, which clearly have shoulders of magnetic origin on their high-energy sides (see Fig. 2). This effect is most likely due to local distortions of the charge distribution caused by the oxygen vacancy concentration δ which is an average quantity, whereas the CEF potential is a local property of each individual Ho^{3+} site. Thus for the CEF problem the chemical formula $HoBa_2Cu_3O_{7-\delta}$ should be rather written as $(HoBa_2Cu_3O_6)_\delta(HoBa_2Cu_3O_7)_{1-\delta}$. $HoBa_2Cu_3O_6$ has the tetragonal D_{4h} symmetry which implies a different CEF splitting pattern compared to the orthorhombic D_{2h} symmetry of $HoBa_2Cu_3O_7$. Since the oxygen degradation mainly occurs in the Cu-O chains, i.e., far away from the Ho^{3+} site, its influence on the CEF potential is expected to be rather small, which has recently been confirmed by comparing the CEF excitation spectra of $TmBa_2Cu_3O_6$ and $TmBa_2Cu_3O_7$.[13] Apart from a minor change in the overall energy scale the major difference between the D_{2h} and D_{4h} symmetries is that the CEF singlet states Γ_2 and Γ_4 of $HoBa_2Cu_3O_7$ merge into a CEF doublet state Γ_5 of $HoBa_2Cu_3O_6$. These differences manifest themselves only in the low-energy part of the observed energy spectra where the resolution is sufficiently high. Indeed we may attribute the high-energy shoulders of peaks B and C to CEF transitions in $HoBa_2Cu_3O_6$, which is furthermore supported by the fact that their intensities amount to about 25% of the main peaks as expected for an oxygen vacancy concentration $\delta\simeq 0.2$.

Nowhere in the observed energy spectra have we been able to perform a detailed study of the linewidths of the CEF transitions versus temperature. The linewidths observed at $T=1.5$ K are throughout slightly broader than

TABLE I. Calculated and experimentally determined coordination factors γ_{2n}^{2m} for the Ho^{3+} site in $HoBa_2Cu_3O_7$. The experimentally determined ratios are the result of combining Eqs. (6) and (8). The sign reversal of some ratios $\gamma_{2n}^{2m}/\gamma_{2n}^{0}$ for oxygen and copper coordination is the result of a rotation of the frame of coordinates by an angle $\phi\simeq\pi/4$ and thus physically insignificant.

		Calculated nearest-neighbor oxygen coordination		Calculated nearest-neighbor copper coordination		Experimentally determined
$2n$	$2m$	γ_{2n}^{2m} (10^{-3} Å$^{-(2n+1)}$)	$\gamma_{2n}^{2m}/\gamma_{2n}^{0}$	γ_{2n}^{2m} (10^{-3} Å$^{-(2n+1)}$)	$\gamma_{2n}^{2m}/\gamma_{2n}^{0}$	$\gamma_{2n}^{2m}/\gamma_{2n}^{0}$
2	0	9.754	1.00	−10.326	1.00	1.00
2	2	3.031	0.31	−2.340	0.23	0.43 ± 0.11
4	0	−5.126	1.00	−0.977	1.00	1.00
4	2	1.250	−0.24	−0.089	0.09	-0.07 ± 0.02
4	4	22.968	−4.48	−6.812	6.97	-4.6 ± 0.2
6	0	0.199	1.00	0.044	1.00	1.00
6	2	−0.044	−0.22	0.009	0.20	-0.6 ± 0.2
6	4	5.243	26.40	−0.613	−13.96	30.0 ± 1.2
6	6	0.045	0.22	0.021	0.48	-0.4 ± 0.2

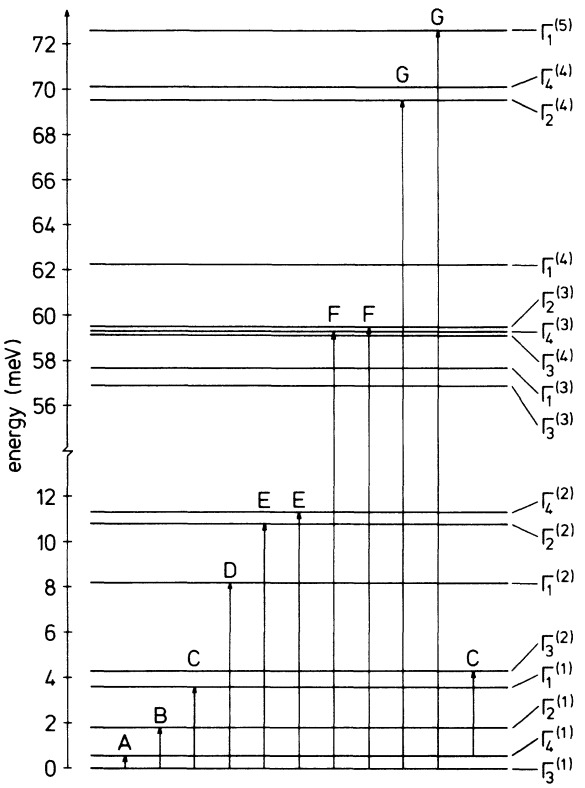

FIG. 6. Energy-level scheme of Ho^{3+} in $HoBa_2Cu_3O_{7-\delta}$ calculated from the CEF parameters of Eq. (8). The arrows denote the observed CEF transitions.

the instrumental resolution, and we estimate the intrinsic linewidths of the CEF transitions to be of the order of 0.5 meV at low temperatures, comparable to the linewidths derived for $ErBa_2Cu_3O_7$.[11] The intrinsic linewidth is most likely due to a static effect resulting from incomplete oxygen occupation in the nearest-neighboring coordination shell as derived from neutron diffraction.[7] Upon raising the temperature all the observed CEF transitions in $HoBa_2Cu_3O_7$ are contaminated by a rapidly increasing number of excited-state CEF transitions as exemplified in Fig. 5, so that a detailed linewidth analysis becomes unreliable. Thus the question of whether the CEF linewidths of $HoBa_2Cu_3O_7$ suffer a sudden drop at T_c similar to $ErBa_2Cu_3O_7$ (Ref. 11) remains open.

V. MAGNETIC PROPERTIES

The CEF parameters (7) may now be used to calculate the magnetic properties of $HoBa_2Cu_3O_7$. The magnetic single-ion susceptibility χ_δ^α ($\alpha = x,y,z$) turns out to be extremely anisotropic as shown in Fig. 7. At low temperatures the x axis is the easy axis of magnetization, but at $T \simeq 100$ K there is a crossover between χ_δ^x and χ_δ^z with a corresponding change of the easy axis of magnetization. The low-temperature anisotropy was recently confirmed by single-crystal magnetization measurements[22] in fields up to 18 T; however, the calculated magnetization values exceed the experimental data by typically 30%, except for low fields ($H < 5$ T) and at low temperatures ($T < 12$ K) where good agreement was achieved. The observed magnetization anomaly for H||z at 80 K cannot be reproduced by our calculations. All these discrepancies are most likely due to incomplete field penetration. On the other hand, our calculations are in rather good agreement with high-field magnetization measurements of a powder sample[23] as shown in Fig. 8. The experimental data do not deviate by more than 10% from the calculated average $\langle M \rangle = (M_x + M_y + M_z)/3$.

Heat-capacity measurements of $HoBa_2Cu_3O_7$ exhibit a peak at $T_m = 0.17$ K indicative of a magnetic phase transition.[24] The transition temperature, however, is so low that the excited CEF states cannot be sufficiently admixed to the ground-state singlet to realize long-range magnetic or-

TABLE II. Wave functions, ground-state transition matrix elements, and energies of the CEF states of Ho^{3+} in $HoBa_2Cu_3O_7$ calculated from the CEF parameters of Eq. (8). The energies of the observed CEF states are also listed.

Γ_i	a_8	a_7	a_6	a_5	a_4	a_3	a_2	a_1	a_0	$\lvert\langle\Gamma_i\rvert J_\perp \rvert\Gamma_3^{(1)}\rangle\rvert^2$	E_{calc} (meV)	E_{obs} (meV)
$\Gamma_3^{(1)}$	0.10	· · ·	0.52	· · ·	0.18	· · ·	0.44	· · ·	0	0	0	· · ·
$\Gamma_4^{(1)}$	· · ·	0.44	· · ·	0.18	· · ·	0.51	· · ·	0.13	· · ·	18.31	0.55	0.5 ± 0.1
$\Gamma_2^{(1)}$	· · ·	0.46	· · ·	−0.04	· · ·	0.53	· · ·	−0.08	· · ·	4.71	1.84	1.8 ± 0.2
$\Gamma_1^{(1)}$	0.36	· · ·	0.11	· · ·	0.59	· · ·	0.07	· · ·	0.06	3.28	3.63	3.8 ± 0.2
$\Gamma_3^{(2)}$	0.36	· · ·	−0.16	· · ·	0.57	· · ·	−0.13	· · ·	0	0	4.33	4.3 ± 0.3
$\Gamma_1^{(2)}$	−0.08	· · ·	0.60	· · ·	−0.10	· · ·	0.34	· · ·	−0.01	11.04	8.15	8.1 ± 0.2
$\Gamma_2^{(2)}$	· · ·	0.05	· · ·	0.66	· · ·	0.04	· · ·	0.23	· · ·	2.73	10.77	10.8 ± 0.4
$\Gamma_4^{(2)}$	· · ·	0.16	· · ·	−0.64	· · ·	0.14	· · ·	−0.21	· · ·	4.14	11.33	11.6 ± 0.4
$\Gamma_3^{(3)}$	0.02	· · ·	0.46	· · ·	−0.01	· · ·	−0.54	· · ·	0	0	56.86	· · ·
$\Gamma_1^{(3)}$	0.50	· · ·	0.01	· · ·	−0.29	· · ·	−0.01	· · ·	−0.57	0.14	57.68	· · ·
$\Gamma_3^{(4)}$	0.60	· · ·	−0.01	· · ·	−0.38	· · ·	0.02	· · ·	0	0	59.16	· · ·
$\Gamma_4^{(3)}$	· · ·	0.34	· · ·	0.21	· · ·	−0.23	· · ·	−0.53	· · ·	0.72	59.25	59.0 ± 0.8
$\Gamma_2^{(3)}$	· · ·	0.32	· · ·	−0.21	· · ·	−0.21	· · ·	0.56	· · ·	1.14	59.46	59.0 ± 0.8
$\Gamma_1^{(4)}$	0.32	· · ·	−0.01	· · ·	−0.24	· · ·	0.03	· · ·	0.82	0.02	62.17	· · ·
$\Gamma_2^{(4)}$	· · ·	0.42	· · ·	0.11	· · ·	−0.42	· · ·	−0.36	· · ·	0.94	69.53	70.0 ± 1.0
$\Gamma_4^{(4)}$	· · ·	−0.41	· · ·	0.12	· · ·	0.41	· · ·	−0.39	· · ·	0.03	70.11	· · ·
$\Gamma_1^{(5)}$	−0.01	· · ·	−0.35	· · ·	0.01	· · ·	0.61	· · ·	−0.04	0.81	72.60	73.0 ± 1.0

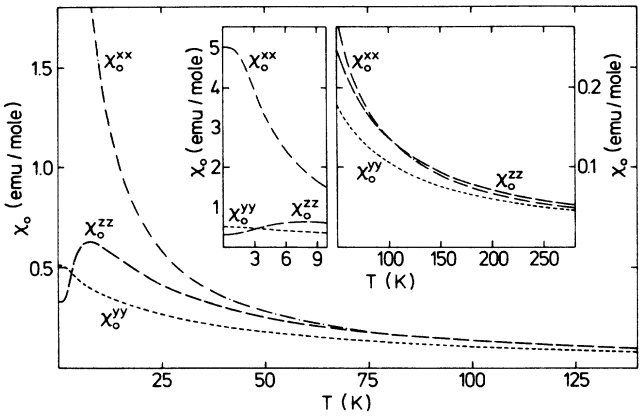

FIG. 7. Magnetic single-ion susceptibility χ_0^{α} of $HoBa_2Cu_3O_7$ calculated from the CEF parameters of Eq. (8).

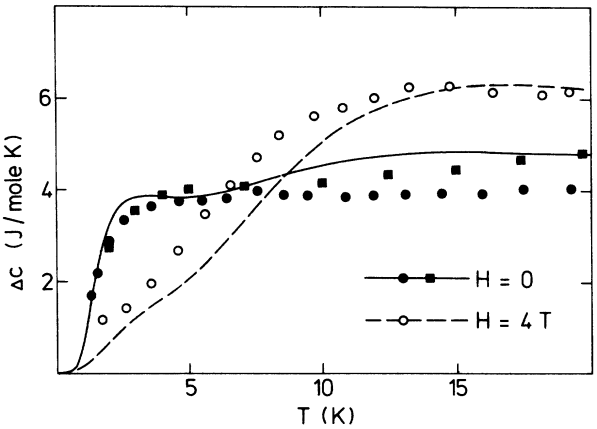

FIG. 9. Schottky anomaly of the specific heat associated with the CEF splitting of Ho^{3+} in $HoBa_2Cu_3O_7$. The solid and open circles correspond to the experimental data of Ref. 25 in zero field and for $H=4$ T, respectively. The squares denote the average of three zero-field data sets (Refs. 24–26). The lines are the results of a calculation based on the CEF parameters of Eq. (8).

dering through a conventional dipolar coupling mechanism. Indeed, a recent neutron-diffraction study of $HoBa_2Cu_3O_7$ demonstrated the absence of long-range magnetic ordering and gave evidence for the onset of two-dimensional antiferromagnetic correlations below $T_m = 0.14$ K.[7]

The Schottky anomaly Δc of the heat capacity offers another possibility to check the reliability of the CEF parameters determined in the present work. A very detailed study of the specific heat in magnetic fields up to 5 T was recently performed by van der Meulen *et al.*[25] Part of their results are shown in Fig. 9 together with our calculations which are in reasonable agreement. Particularly, the shape of the Schottky anomaly in zero field and for $H=4$ T is nicely reproduced. We do not expect to obtain perfect quantitative agreement between the calculated and observed heat-capacity data, since the latter are the result of a correction procedure which takes account of the electronic and phonon contributions. Such correction procedures have to be considered with caution; indeed in two other publications[24,26] Schottky heat-capacity data were reported which are either slightly below[24] or drastically above[26] the observed zero-field data of Ref. 25. Nevertheless, it is interesting to notice that we obtain almost perfect agreement between our calculation and the average of the three observed data sets[24–26] as shown in Fig. 9.

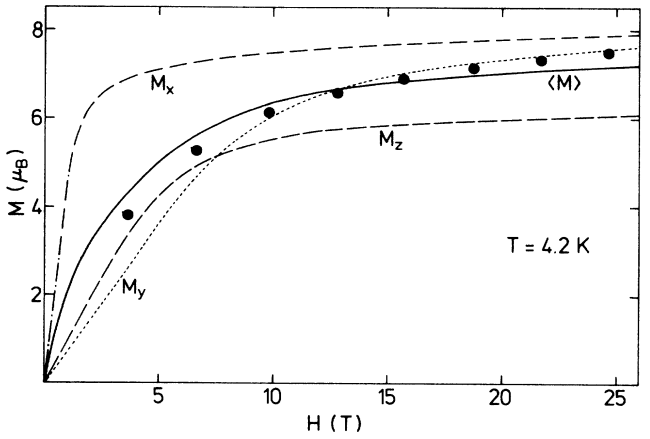

FIG. 8. High-field magnetization of $HoBa_2Cu_3O_7$. The circles denote the experimental data taken for a polycrystalline sample (Ref. 23), and the lines are the results of a calculation based on the CEF parameters of Eq. (8).

VI. CONCLUSIONS

We have been able to unambiguously determine all nine CEF parameters of Ho^{3+} in $HoBa_2Cu_3O_7$ with use of the INS technique. Clearly, the CEF parameters derived by Mirmelshtein *et al.*[12] from neutron spectroscopy are inadequate, since the CEF excitations into the high-energy window were not taken into account. The reliability of our CEF parameters is supported by the good agreement between the calculated and observed magnetization and Schottky heat-capacity data of $HoBa_2Cu_3O_7$. The comparison of the field-dependent properties turned out to be particularly useful, since the external field predominantly probes the wave functions of the CEF states.

We emphasize the role of neutron spectroscopy among all experimental techniques as a unique and powerful tool to determine the CEF interaction in the low-symmetry $RBa_2Cu_3O_7$ compounds. Any attempts to unravel the complicated CEF level structure in these systems from the bulk properties are likely to fail as exemplified for $HoBa_2Cu_3O_7$ in Ref. 26.

A relatively simple understanding of the CEF parameters may result from a calculation which takes account of the neighboring coordination polyhedra around the Ho^{3+} ions. The CEF parameters are then given by

$$B_{2n}^{2m} = a_{2n}^{2m} \langle r^{2n} \rangle \chi_{2n} \gamma_{2n}^{2m} , \tag{9}$$

where $\langle r^{2n} \rangle$ is the $2n$th moment of the radial distribution of the $4f$ electrons, χ_{2n} is a reduced matrix element, and a_{2n}^{2m} is a reduced CEF parameter. In the simple point-charge model we expect constant values $a_{2n}^{2m} = Ze^2$, where Z is the charge of the coordinating ion in units of the elec-

tron charge $|e|$. This simple model, however, completely fails. From the CEF parameters B_2^0, B_4^0, and B_6^0 we derive effective charges $Z=+0.7$, $+2.6$, and $+6.2$ for oxygen coordination and $Z=-0.6$, $+13.7$, and $+27.9$ for copper coordination, respectively. In other words, the point-charge model predicts neither the sign nor the size of the CEF parameters correctly. On the other hand, the experimentally determined ratios $\gamma_{2n}^{2m}/\gamma_{2n}^{0}$ are in reasonable agreement with the calculated values for nearest-neighbor oxygen coordination as shown in Table I, which means that Eq. (6) is indeed a good approximation to describe the CEF potential in $HoBa_2Cu_3O_7$. For nearest-neighbor copper coordination there are large discrepancies particularly for the ratios γ_4^4/γ_4^0 and γ_6^4/γ_6^0 which decisively control the relative distribution of CEF levels. Obviously the CEF interaction in $HoBa_2Cu_3O_7$ is mainly determined by the charge distribution of the nearest-neighboring oxygen shell.

Our results obtained for $HoBa_2Cu_3O_7$ may easily be used to extrapolate the CEF interaction to other $RBa_2Cu_3O_7$ compounds, since the CEF is not controlled by the rare-earth ion but by the coordination polyhedra which are known to be unaffected by the rare-earth ions in these systems.[24] Therefore we may anticipate constant values of the reduced CEF parameters a_{2n}^{2m} defined by Eq. (9) through the whole rare-earth series. Recently, Walter *et al.*[11] have performed INS experiments for $ErBa_2Cu_3O_7$ and derived part of the CEF level scheme. Extrapolating the CEF level scheme from our $HoBa_2Cu_3O_7$ data to $ErBa_2Cu_3O_7$ yields good agreement (typically within 10%) with the experimental data.[11] However, we have shown[15] that Walter *et al.* have not been able to correctly assign the excited-state CEF transitions, and thereby arrived at an incorrect CEF splitting pattern.

The most important issue of the present work is the fact that we have been able to determine the magnetic ground state of $HoBa_2Cu_3O_{7-\delta}$. This is necessary information in forthcoming studies of the interplay of magnetism and superconductivity in the perovskite-type superconductors, similar to the rare-earth compounds RM_6X_8 (X=S,Se) and RRh_4B_4 which also exhibit a coexistence between magnetism and superconductivity at low temperatures.[27]

ACKNOWLEDGMENTS

Discussions with Dr. P. Fischer are gratefully acknowledged. We also should like to thank Dr. R. Marsolais for performing thermogravimetric measurements. This research was partly supported by the Swiss National Science Foundation.

[1] J. G. Bednorz and K. A. Müller, Z. Phys. B **64**, 189 (1986).
[2] M. K. Wu, J. R. Ashburn, C. J. Torng, P. H. Hor, R. L. Meng, L. Gao, Z. J. Huang, Y. Q. Wang, and C. W. Chu, Phys. Rev. Lett. **58**, 908 (1987).
[3] P. H. Hor, R. L. Meng, Y. Q. Wang, L. Gao, Z. J. Huang, J. Bechtold, K. Forster, and C. W. Chu, Phys. Rev. Lett. **58**, 1891 (1987).
[4] M. B. Maple, K. N. Yang, M. S. Torikachvili, J. M. Ferreira, J. J. Neumeier, H. Zhon, Y. Delichaouch, and B. W. Lee, Solid State Commun. **63**, 635 (1987).
[5] F. Hulliger and H. R. Ott, Z. Phys. B **68**, 291 (1987).
[6] J. W. Lynn, W. H. Li, Q. Li, H. C. Ku, H. D. Yang, and R. N. Shelton, Phys. Rev. B **36**, 2374 (1987).
[7] P. Fischer, K. Kakurai, M. Steiner, K. N. Clausen, B. Lebech, F. Hulliger, H. R. Ott, P. Brüesch, and P. Unternährer, Physica C **152**, 145 (1988).
[8] D. McK. Paul, H. A. Mook, A. W. Hewat, B. C. Sales, L. A. Boatner, J. R. Thompson, and M. Mostoller, Phys. Rev. B **37**, 2341 (1988).
[9] A. I. Goldman, B. X. Yang, J. Tranquada, J. E. Crow, and C. S. Jee, Phys. Rev. B **36**, 7234 (1987).
[10] U. Walter, S. Fahy, A. Zettl, S. G. Louie, M. L. Cohen, P. Tejedor, and A. M. Stacy, Phys. Rev. B **36**, 8899 (1987).
[11] U. Walter, E. Holland-Moritz, A. Severing, A. Erle, H. Schmidt, and E. Zirngiebl, Physica C (to be published).
[12] A. V. Mirmelshtein, A. A. Podlesnyak, V. I. Bobrovskii, S. A. Davydov, A. E. Karkin, V. L. Kozhevnikov, S. M. Cheshnitskii, and B. N. Goshchitskii, Physica C (to be published).
[13] E. Gering, B. Renker, H. Schmidt, M. Bonnet, F. Gompf, D. Ewert and A. Dianoux, Physica C (to be published).
[14] M. Bonnet, E. Gering, M. J. G. M. Jurgens, J. Y. Henry, J. Rossat-Mignod, R. Calemczuk, and E. Bonjour, Physica C (to be published).
[15] A. Furrer, P. Brüesch, and P. Unternährer, Physica C (to be published); Solid State Commun. **67**, 69 (1988).
[16] K. Kishio, J. Shimoyama, T. Hasegawa, K. Kitzawa, and K. Fueki, Jpn. J. Appl. Phys. **26**, L1228 (1987).
[17] P. Brüesch and W. Bührer, Z. Phys. B **70**, 1 (1988).
[18] G. T. Trammell, Phys. Rev. **92**, 1387 (1953).
[19] K. W. H. Stevens, Proc. Phys. Soc. London, Sect. A **65**, 209 (1952).
[20] K. R. Lea, M. J. M. Leask, and W. P. Wolf, J. Phys. Chem. Solids **23**, 1381 (1962).
[21] M. T. Hutchings, in *Solid State Physics,* edited by F. Seitz and D. Turnbull (Academic, New York, 1964), Vol. 16, p. 227.
[22] J. L. Tholence, H. Noel, J. C. Levet, P. Gougeon, G. Chouteau, and M. Guillot, Physica C (to be published).
[23] L. W. Roeland, F. R. de Boer, Y. K. Huang, A. A. Menovskii, and K. Kadowaki, Physica C **152**, 72 (1988).
[24] B. D. Dunlap, M. Slaski, D. G. Hinks, L. Soderholm, M. Beno, K. Zhang, C. Segre, G. W. Crabtree, W. K. Kwok, S. K. Malik, I. K. Schuller, J. D. Jorgensen, and Z. Sungaila, J. Magn. Magn. Mater. **68**, L139 (1987).
[25] H. P. van der Meulen, J. J. M. Franse, Z. Tarnawski, K. Kadowaki, J. C. P. Klaasse, and A. A. Menovsky, Physica C **152**, 65 (1988).
[26] J. M. Ferreira, B. W. Lee, Y. Dalichaouch, M. S. Torikachvili, K. N. Yang, and M. B. Maple, Phys. Rev. B **37**, 1580 (1988).
[27] See, for example, *Superconductivity in Ternary Compounds II,* edited by M. B. Maple and O. Fischer (Springer, Berlin, 1982), and references therein.